Point-spread Analysis of γ-ray/depth Spectra for Borehole Monitoring Applications

Soraia C. Elísio, Aliyu Bala, Manuel Bandala, James Graham, Alex Grievson and Malcolm J. Joyce (*Member, IEEE*)

***Abstract*—An approach to the analysis of γ-ray spectra that might arise as depth profiles from the characterization of radioactivity in boreholes is described. A borehole logging probe, 'ABACUS', has been designed and constructed which comprises a cerium bromide detector and a built-in multichannel analyzer. This has been tested in a bespoke, laboratory-based testbed built to replicate the borehole environment. An established, semi-empirical model has been applied data arising from the cerium bromide scintillation detector to extract the number of counts under the photopeak from each of the resulting γ-ray spectra (in this case the 662 keV line from ^{137}Cs) associated with each depth position, and which also enables this information to be isolated from other contributions such as background and the Compton continuum. A complementary approach has been adopted to process the asymmetric and non-Gaussian trend that concerns the photopeak count as a function of depth in the borehole testbed for a given depth profile, when the testbed is subject to the activity provided by a sealed, ^{137}Cs source. This comprises a modified, Moffat point-spread function. The Moffat function is a continuous probability distribution based upon the Lorentzian distribution. Its particular importance is due to its ability to reconstruct point spread functions that comprise wings that cannot be reproduced accurately by either a Gaussian or Lorentzian function. This application of the Moffat formalism to radioactive contamination assessment profiles enables an effective and accurate assessment to be made of the position of localized radioactivity in the testbed wall.**

***Index Terms*—Radioactive pollution, γ-ray detection, Gaussian distribution, curve fitting, nuclear measurements.**

I. Introduction

SOME facilities used for the interim storage of spent nuclear fuel, i.e., ponds and wet silos, were not designed to modern standards and, consequently, radioactivity has leaked from them to ground [1]. This migratory contamination poses a risk to groundwater, public health, and the environment. As a consequence, investigations are necessary to locate it in order to better understand its transport and fate, the associated radiological risk and to inform site remediation programs.

Often, best practice to assess such situations includes the installation of monitoring wells or boreholes to enable groundwater sampling campaigns and subsequent radiological analysis. Such boreholes usually extend into the ground to intersect the groundwater table and can have, for example, a slotted screen section at a specific depth to allow the water to flow in. Samples are then collected from these penetrations and sent for laboratory analysis; the latter can comprise purification to isolate a target radionuclide followed by spectroscopy.

However, such sampling can be laborious and can result in secondary wastes whereas, in areas with high dose rates, it can present radiological risks that might be avoided otherwise; neither is it ideal where wells are susceptible to drying out as the opportunity for sampling can then be lost.

Borehole logging is an alternative to sampling to assess radioactivity in the ground, and has the potential to provide an in-situ, continuous and real-time assessment of radioactive source distributions. In this context, logging might comprise recording ionizing radiation characteristics as a function of depth in a monitoring well. However, since it was pioneered for geophysical prospecting [2] most reported works have focused on an *active* application in which radioactivity is used as a tool rather than being the objective of the assessment. The *passive* assessment of land contaminated with radioactivity via boreholes has received less attention, with works focusing on for example: the correlation between measurements made on core samples and in boreholes [3]; spectral-shape distinction of caesium-137 and cobalt-60 [4]; high-resolution logging systems [5][6] and the analysis radial distributions of cobalt-60 from buried corrosion [7].

Passive borehole measurements can be made either by stepwise recording, whilst a measurement probe is stationary at selected depths (such as at the water table level for example), or by lowering the probe gradually into a well. In the former, the probe is in direct contact with contamination that might be entrained within water in the well; in the latter, the contamination is present in the ground (or within ground-fluids) surrounding the borehole and does not have to be in direct contact with the probe. However, several limitations remain concerning, for example, the easy recovery of energy spectra with depth information that is accurate and consistent.

This paper describes the design and test of a logging probe [8] and an associated method to infer the depth of a source of radiation in a borehole environment. A computer-implemented method to locate radioactivity in blind tubes is presented that combines the direct detection of the caesium-137 photopeak

This research is supported by the National Nuclear Laboratory (NNL) and Sellafield Ltd. (UK) via the EPSRC programme "TRANSCEND", (TRANSformative Science & Engineering for Nuclear Decommissioning), code EP/S01019X/1. M. J. J. acknowledges the support of the Royal Society via a Wolfson Research Merit Award.

S. Elísio (s.elisio@lancaster.ac.uk), M. Bandala and M. J. Joyce (m.joyce@lancaster.ac.uk) are with the School of Engineering, Lancaster University, LA1 4YW, UK.

A. Bala and A. Grievson were with Hybrid Instruments Ltd., Lancaster, LA14YW, UK. A. Bala is now with Createc Ltd., Cockermouth, Cumbria, UK.

J. Graham is with the NNL, Cumbria, UK.

with an application of an astrophysical seeing formalism. This is used to derive individual radioactivity depth profile trends and, hence, to enable an estimate for the depth of isolated radioactivity in a laboratory-based, borehole analogue to be extracted.

II. Background

The radiation detected with in-situ detector probes in boreholes on land contaminated by products of the nuclear fuel cycle usually comprises γ rays (due to their characteristic penetrative strength and the prominent yield of γ-emitting fission products such as caesium-137) and X-rays by way of bremsstrahlung from high-energy β particles from the decay of prominent β-emitters, such as strontium-90. These photons contribute to characteristic, energy-specific lines in a spectrum (photopeaks), the Compton background because of scattering and the lower-energy X-ray region due to bremsstrahlung.

The volume investigated in-situ approximates typically to a sphere centered on the sensitive volume of the detector in use. The radius of this sphere (corresponding to the depth of investigation) varies with photon energy and the interaction properties of the associated media, i.e., reducing with decreasing photon energy and increasing atomic number of the intervening media. The finite size of the detector may introduce variance from this spherical approximation, and it is anticipated that the properties of the materials constituting the monitoring system and borehole structure can influence the detected bremsstrahlung yield.

Sensors used in logging probes have included gas-filled detectors (Geiger-Müller tube – GM), scintillators (such as thallium-doped sodium iodide – NaI:Tl) and semiconductors (i.e., high-purity germanium detectors – HPGe), yielding a range of capabilities from pulse-counting through to spectroscopy. The data from a deployment are often presented as a γ-ray depth profile in terms of dose intensity, i.e., total counts, or the proportion of the total γ radiation detected associated with a particular energy (and therefore a specific radionuclide) as a function of depth in the ground, where spectroscopy allows.

γ-ray spectroscopy data accrued as a function of depth are generally more complex than dose or gross count data since they contain more detailed information. This might comprise a first profile based on a total γ-ray log (the sum of all type of radiation contributions) and a second profile of calculated abundancies associated with the radiation from each isotopic contribution. Such a dataset might provide information about spatial distributions of leaks in the ground as a function of depth. The output data can also be presented as a time series, where the logging probe is fixed at a specific depth, recording at different times of the year. These data may provide information about, for example, the temporal flow of a radioactivity migrating in the vicinity of the borehole. A space-time compilation of datasets, as well as measurements with an array of monitoring wells, can be essential to monitor local and site-wide mobilization or the remobilization of leaks.

Often, downhole γ-ray logging surveys are conducted in blind tubes which, although having advantages over sampling methods that require subsequent laboratory analysis, can be challenging due to deployment constraints, limitations of the sensing apparatus and radiological restrictions, where they arise. For example, long-established boreholes on some nuclear sites can be lined with carbon steel and can have screen depths of up to 10 m below ground level. They are often blinded (that is, end-capped and thus sealed) to ensure that direct contact of the probe with the contamination surrounding the blind tube is prevented. Whilst desirable operationally, this arrangement complicates the detection of radiations from α- and β-emitting radionuclides (notwithstanding the potential for bremsstrahlung from the latter). Further, a typical tube radius of ~75 mm can limit the range of probes that will fit, recognizing that some radial margin is essential given the imperative that probes do not become stuck whilst in use.

Anthropogenic radioactivity in the ground is often dominated by caesium-137 and strontium-90, and the latter's daughter, yttrium-90. Hence, a system providing dual detection and discrimination of these radionuclides via their photon spectra can have advantages over dose-rate-only datasets. Empirical fitting procedures can be necessary to extract such spectroscopic features consistently across many spectra, and to extract the corresponding depth of contamination from the depth profile: this is the focus of this work.

III. Method

A. Photopeak fitting

γ-ray spectra arising from measurements in boreholes can require a model to cater for contributions comprising, for example, a *first* source of radiation that can be somewhat discrete (the predominant radionuclide) and a *secondary*, more continuous contribution representative of a relatively complex background.

Caesium-137 is relatively straightforward to quantify given its 662 keV photopeak; a region-of-interest (ROI) in the energy spectrum can be selected between lower L and an upper U energies defined to encompass this. The number of counts within this region is obtained by summing the counts in this histogram, or (better) by fitting and integrating the mathematical function that best describes it. The latter is usually a Gaussian, depending on the complexity of the spectrum.

In addition to the contributions to γ-ray spectra that arise due to photoelectric absorption and the incomplete interactions of photons subsequently escaping the detector crystal, bremsstrahlung arising from β-particle interactions in a steel blind-tube liner might also be characterised.

The semi-empirical model applied previously for peak-shape analysis of multichannel pulse-height spectra from high-resolution germanium γ-ray detectors [9][10][11][12] has been adopted here to describe and quantify spectra in the vicinity of a peak from a cerium bromide ($CeBr_3$) scintillator, as per the function, f, represented by a sum of terms defined below,

$$f(x) = G(x) + S(x) + T(x) + \mathrm{b} \quad (1)$$

where x is the abscissa corresponding to photon energy, $G(x)$ the Gaussian function representing the photopeak, $S(x)$ represents a step discontinuity that may appear in the continuum below the Gaussian peak on its low-energy side, $T(x)$ represents the exponential trend in counts that may appear in the continuum below the Gaussian peak, again, on its low-energy side and b is an offset corresponding to the residual background level.

$G(x)$ is defined (2) where A is the amplitude of the Gaussian function, μ is the mean and σ the standard deviation,

$$G(x) = \mathrm{A}e^{-\frac{(x-\mu)^2}{2\sigma^2}} \tag{2}$$

$S(x)$ is defined as per (3) where B is the step function amplitude (expressed as a fraction of A), $\mathrm{erfc}(x)$ is the complementary error function and the tail function, $T(x)$, is as per (4), where C is the tail function amplitude (expressed as a fraction of A), and m is the slope of the exponential,

$$S(x) = \mathrm{AB}\ \mathrm{erfc}\left(\frac{x-\mu}{\sigma\sqrt{2}}\right) \tag{3}$$

$$T(x) = \mathrm{AC}e^{\frac{x-\mu}{\mathrm{m}\sigma}}\ \mathrm{erfc}\left(\frac{x-\mu}{\sigma\sqrt{2}} + \frac{1}{\mathrm{m}\sqrt{2}}\right) \tag{4}$$

The contribution due to the principal radionuclide over a complex continuum background of radiation is then calculated using (5), where N is then the number of counts corresponding to the photopeak, obtained by calculating the area under the Gaussian, $G(x)$,

$$\mathrm{N} = \int_{\mu-\mathrm{n}}^{\mu+\mathrm{n}} G(x)dx \tag{5}$$

wherein n assumes a predetermined constant value indicative of a photon-energy interval sufficient to cover 3σ either side of the photopeak, and the uncertainty in the N measurement is obtained by error propagation considering the obtained standard deviation in the fitted variables (from the covariance matrix).

B. Modelling γ-ray log depth profiles

The response of a γ-ray logging tool can be represented as the total number of detected γ-ray counts due to the γ-emitting radioactive material present in the volume of investigation, or in terms of the constituent proportions derived from analysis of a corresponding γ-ray spectrum. The contribution of individual isotopes can be evaluated and plotted as a function of depth from this analysis, yielding depth profiles for specific γ-ray lines.

Typically, a pulse function can be used to represent the variation in response intensity of the logging γ-ray tool as a function of depth in the vicinity of a radioactive anomaly in the ground. This can be interpreted in terms of the hypothetical response of a point-detector at an infinitely-slow logging speed (depth series) for a uniform zone of contamination. However, the boundaries of a pulse may not be defined sharply and pulses may have irregular shapes due to factors such as logging speed and measurement time, the size of the sensitive volume of the detector, variation of the spatial distribution of the source radioactivity in the bed formation and changes in the volume of investigation from one measurement to another.

Logging tools are often used in boreholes in radioactive areas to locate contamination zones and to determine the distribution of migrating radioactivity from a source, as well as to identify and obtain relative proportions of specific nuclides within a given medium. These objectives can require careful analysis of the overall shape of the depth profile in specific regions where changes in intensity, corresponding to radioactive anomalies, are to be resolved to a sufficient degree.

Changes in shape of the intensity profile can be due to a combination of influences such as changes in activity, source dispersion, and the geometry of shielding materials. A source of radiation in a medium can be theorized as an extended homogeneous layer with a notional volume (extended depth vertically and horizontally relative to the orientation of the borehole), or as a point source (such as a 'hot' particle) at a vertical/horizontal position to the borehole), as well as heterogeneous sources comprised of various point sources at different positions but within a defined volume [4]. In practice, the distribution of radioactivity in the ground is often complex and may comprise several configurations.

A scenario approximating to a point source in the ground, assessed with a single transit of logging system across a range in depth spanning the position of the source, might yield a single peak-shape that can be described by simple model with a small number of fitting parameters. A one-dimensional, point-spread function (PSF) is an attractive option for the analysis of discrete photon-depth spectra profiles of a point source near to a blind-tube. However, such a function should encompass the entire activity profile including an inner zone (corresponding to the core of the profile) and an outer zone with low numbers of counts present in its 'wings'. Whilst a Gaussian distribution might serve as a first approximation, the extremities of a profile can be more extensive than this is able to fit self-consistently. This introduces important uncertainties as to the depth at which a radioactive anomaly is discernible from the ambient.

An alternative to a Gaussian is the Moffat peak-like distribution because this accounts for the departure from Gaussian shape in the extremities either side of the peak. A Moffat distribution is a Lorentzian continuous probability distribution modified with a variable power index. It is often described as a special case of the multivariate student-t distribution, specifically a distribution of a bivariate random variable (x, y) centered at zero (or as of the corresponding radius in this context). It has been used in astrophysics applications [13] to cater for seeing effects (see below) in stellar profiles and for synapse image analysis concerning the non-uniform scattering of photons across the brain/cranial window of mammals [14].

In astronomy, 'seeing' refers to image degradation of an astronomical object caused by atmospheric turbulence [13]. This results in brightness distributions (or radial intensity profiles) in captured, 2D, ground-based images. Such abnormal radial intensities can manifest as irregular wings in the point-spread profiles that neither Gaussian nor Lorentzian distributions reproduce consistently, whereas a Moffat PSF can.

The standard, 2D, Moffat PSF characterises a spatial distribution of photons under the assumption of circular symmetry, i.e., a circular aperture, centred at the object centroid, as per g, where,

$$g(x,y) = \mathrm{I}\left[1 + \frac{(x-p_x)^2}{\mathrm{w}_x^2} + \frac{(y-p_y)^2}{\mathrm{w}_y^2}\right]^{-\beta} \quad (6)$$

where x, y in this context denote position, I is the amplitude and p_x, p_y denote the centroid position of the profile in the image. The parameters w_x, w_y and β account for the effect of photon scattering in a medium between the object and the detector recording the image, often referred to as *seeing parameters* that govern the width and the shape of a profile, respectively: w is a scale parameter that determines the width of the distribution and radius of a circle ($\mathrm{w} = \mathrm{w_x} = \mathrm{w_y}$) in a 2D image projection as per figure 1A; β parameterizes the extent of the wings either side of the peak of the distribution, correcting the anomalous slope for larger radii. Note: larger values of β result in a steeper slope and, when $\beta \to \infty$, the function tends to a Gaussian. Radii in one axis projection can be calculated from the full-width-at-half-maximum as equal to $\frac{FWHM}{2} = 2\mathrm{w}\sqrt{2^{1/\beta} - 1}$, or the full-width-at-tenth-maximum as equal to $\frac{FWTM}{2} = 2\mathrm{w}\sqrt{10^{1/\beta} - 1}$, based on the chosen percentage of the amplitude signal (desired level of significance). The parameter β influences the resulting radius.

Population studies of dense stellar fields have proposed the use of modified 2D Moffat PSFs because the spatial brightness of these distributions exhibits a degree of asymmetry. Analytically, this arises because, for elliptical dispersion, the parameter width is no longer equal for *x*- and *y*-projections (and thus $\mathrm{w}_x \neq \mathrm{w}_y$), as per figure 1B, where the semi-major and other the semi-minor axes ($\mathrm{w_x}, \mathrm{w_y}$) are referenced to the central coordinates of the corresponding ellipse (x_0, y_0). The FWHM varies symmetrically for each axis projection and at any specific inclination angle with the *x*-axis [15]. Asymmetry in a single axis projection can be introduced via a position-dependent function in the corresponding width parameter, $\mathrm{w_x}$ given by a sigmoid-type function $\mathrm{s}(x) = 2\mathrm{w}_x/\left(1 + e^{\gamma(x-\mathrm{x_0})}\right)$ for *x*-axis asymmetry (on the *y*-axis the profile is symmetrical). This asymmetric, 2D, Moffat PSF represents a complex non-elliptical object [16] (see figure 1C) where $\mathrm{w}_x \neq \mathrm{w}_y$, and γ regulates the skewness of the peak profile.

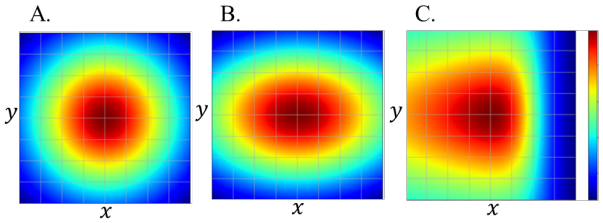

Fig. 1. A computer-generated images with colour schemes representing the varying intensity levels across (*x,y*) coordinates for A. symmetrical, B. elliptical, and C. asymmetric 2D Moffat PSFs.

Considering the photon dispersion depth profile of a vertical, one-dimensional scan of the simplest, point radioactive source distribution, a one-dimensional PSF is sufficient. Any eccentricity in the wings (corresponding to a contaminated zone boundary) is characterised by a Moffat PSF; any asymmetry is accounted for via an additional factor to yield a revised expression for g, as per,

$$g(x) = \mathrm{I}\left[1 + \frac{(x-p_x)^2}{\left(\frac{2w_x}{1+e^{\gamma(x-p_x)}}\right)^2}\right]^{-\beta} \quad (7)$$

where γ can be positive or negative, to indicate skew to the lower and higher values of a depth maximum, respectively, and null if symmetric, with β and w_x defined as positive. Higher values of β indicate a higher slope of the distribution wings, and higher values of w_x indicate a wider distribution. Note: The calculation of FWHM is more complex in non-symmetric cases, as an explicit isolated solution for $(x - p_x)$, and determination of the radius (in a x-axis projection) requires the application of numerical methods, such as the Newton-Raphson method [17]. However, in instances where the fit yields a very small γ value, the previous FWHM expression can be employed for a quick assessment of the spread. This simplified scenario is used to define baseline values for γ, β and w_x. Any detraction from these might be suggest an extended or multicomponent source of radioactivity, or discrepancies due to photon scatter arising due to density or structural changes of the ground surrounding a given borehole.

IV. Materials and Methods

A. *The blind-tube logging probe (BLP) prototype*

The BLP used in this work, 'ABACUS', as per Fig. 2, comprises a γ-ray spectrometer and a digital multi-channel analyser (MCA) in an outer, cylindrical case. The spectrometer is made up of an inorganic scintillation detector and a silicon photomultiplier (SiPM) in a cylindrical, compact (physical size of Ø1.5 x 6.5 cm^2) hermetic unit (VS-1402-20, commercialised by Scionix, Netherlands). The scintillator is a Ø9.5 x 10 mm^2 $\mathrm{CeBr_3}$ crystal, and the crystal readout is a 6 x 6 mm^2 PM6660-SiPM (Ketek GmbH, Germany). The SiPM output is conditioned by a built-in preamplifier to cater for the effect of temperature; the influence of temperature on its light output was not catered for recognising that the measurements were performed in a laboratory with some temperature compensation. Cerium bromide provides competitive γ-ray detection efficiency (with effective atomic number, Z_{eff}, of 46, and density of the material, ρ, of 5.2 $\mathrm{g/cm}^3$), energy resolution (3.2-4% @ 662 keV), high count-rate capability (decay time=17 ns) and radiation hardness (<10^5 Gy) [18].

The MCA used in ABACUS is a Topaz-SiPM supplied in a rugged, and pocket-size (physical size of 7 × 4.5 × 2.6 cm^3) aluminium box with input and output connectors (commercialised by BrightSpec NV). It is amongst the smallest, full-featured MCAs currently available and performs pulse height analysis of the signal from the scintillation detectors to provide energy spectra. It operates on a 5V low-ripple, low-noise supply for the detector and can be interfaced to a laptop or notebook easily via USB 2.0 communication interface for power supply and data transfer. The unit includes a spectroscopy software interface. Note: by installing the MCA

unit in the probe case, the detector output signal is digitalized before being sent to the surface, enabling signal transmission with less noise, distortion, and environmental interference [9].

The probe case has a simple cylindrical geometry and physical dimensions compatible with the dimensions of existing blind tubes. The γ-ray spectrometer is fixed parallel to the central axis of the case and centred at the bottom. A collimator is not used and hence the detection response is assumed isotropic apart from the top side of the crystal where the electronics is housed. The signal processing module is placed on top of the detector and connected to it via a LEMO® connector. The case is made of plastic (Ø 70 × 211 mm long) with a top lid with a hole for the USB cable and a hook to aid deployment and recovery when in use.

B. The deployment system

A typical deployment system for the ABACUS probe comprises a winch by which the tool is lowered and retrieved, a sheave to add change of the direction of the cable between the winch and the hole, and a high-resolution encoder for depth measurement. Typical logging cables (multicore wired) provide a combined means of data transfer, power supply and mechanical support. Surface instruments, comprising a data logger or control unit, store the data and are used to control the winch system, to set the position of the probe within a borehole.

In the context of this work, a simplified deployment system has been used for laboratory-based tests in which a sheave and encoder are not used, with the probe lowered/raised manually with depth position measured using a hand-held, laser-based distance meter at the top of the blind tube. The logging cable consists then of two separate cables: a rope to support the weight of the probe and a 3-m long USB cable for data transmission and power supply.

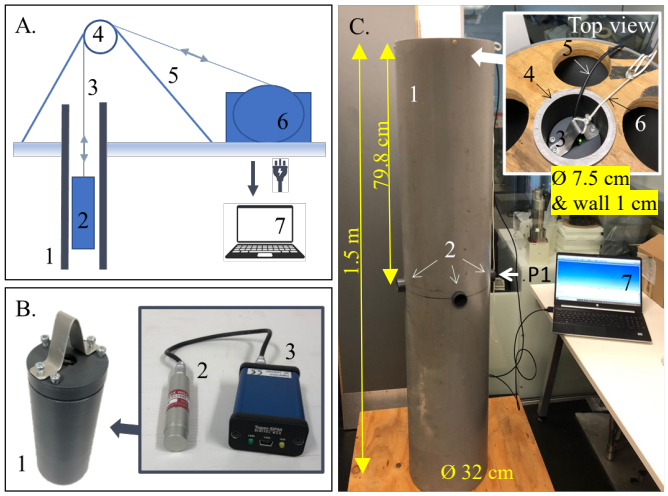

Fig. 2. A. A schematic diagram of the approach showing the borehole (1), the probe (2), and tether (3), the pulley unit of the deployment system (4,5) and the winch (6) and laptop (7). B. The ABACUS probe unit (size Ø7 × 20 cm) (1) including the detector (size Ø1.5×6.5 cm) (2) and MCA (size 7 × 4.5 × 2.6 cm) (3) and C. The laboratory set-up including the testbed (1), the source ports (2) and the top view of the unit.

C. The blind-tube testbed

The blind-tube test bed used in this research is a laboratory-controlled monitoring well designed for radiation detection and photon depth profile testing. It has been designed to calibrate the BLP response for a variety of scenarios (for example, simple-to-complex spatial distributions of source and media) before conducting field measurements.

The testbed comprises an inner, vertical pipe at the centre of an outer pipe fixed in a base, with four smaller tubes intersecting both pipes horizontally, fixed 80 cm from the top. The inner pipe represents the blind tube in this arrangement with the material and size of this pipe selected to replicate legacy blind tubes at nuclear sites, i.e., Sellafield, as close as possible; in this case, blind tubes lined with carbon steel with inner diameters ranging from 75 to 80 mm and wall thicknesses ranging from 6 to 10 mm. The carbon steel tube (European Tubes Ltd., UK) is 1.5 m long with an inner diameter of 75 mm and wall-thickness of 9.5 mm. The outer pipe functions as a material retainer or tank. It is 1.5 m long, 320 mm in diameter, made of plastic and is designed so that the space between the blind tube and the plastic outer pipe can be filled with material (such as sand) to recreate a vertical ground core, translating to about 113 mm of material surrounding the blind tube (not done in this work). The horizontal tubes create a void in the matrix material to enable sealed radioactive sources to be inserted and removed, quickly and easily.

In this research, a scenario has been assumed comprising a single point source with the least degree of scattering possible between source and detector, with the test pit is left empty of material and a sealed source fixed close to the wall of the blind tube.

D. The experimental method

A caesium-137 source with an activity of 304 kBq was inserted into the horizontal tube at position P1 (see Figure 2). The BLP prototype was then lowered into the blind-tube test bed (described above) and fixed at various depth positions using a rope attached to the top of the test bed. The position of the probe in the pipe, d, relative to the top of the test bed, was determined using a hand-held laser position meter. The meter was placed on top of the tank, with its laser output directed downward towards the top surface of the logging probe.

These data were then converted into distance, D, between the top of the pipe and the centre of the sensor element by considering the internal dimensions of the probe. Each spectrum was acquired for one hour to achieve sufficient statistical precision for peak evaluation. The data were transferred via USB 2.0 to a laptop running the γ-ray spectroscopy software, and each spectrum saved in text file format. The following sections describe an algorithm written in python™ used to analyse each obtained spectrum for a variety of depth positions.

E. γ-ray spectral log analysis

The analysis was divided into two stages: The photopeak model (1) is used first to characterise the γ-ray spectra recorded by the BLP. Each spectrum is the energy distribution of the photons (γ rays and X-rays) determined at a specific depth within the blind-tube test bed as per Figure 3; second, the depth profile fit is performed as per Figure 4.

The photopeak model has been applied to each spectrum for each depth position, i, where increasing values of i correspond to increasing depth into the ground or, in this case, the testbed.

A region-of-interest (ROI) defined between a lower L and upper U energy bounds is selected to initialise the method encompassing a photopeak, i.e., the 662 keV line of caesium-137. Initial U and L values were derived from a typical spectrum: L to the right of the Compton edge and U to the right of the photopeak where the count level approaches the level of background noise.

Least-squares minimisation was used to optimise the fit of f (Equation 1) to the data within the ROI at each depth i. The fitting algorithm starts with an initial fitting iteration to obtain initial values for the fit parameters (derived from a typical spectrum) and this is then optimised to obtain the parameters and their associated uncertainties. These values are saved, and the process repeated for the next position. The method checks for errors in the fitting process (such as a failure of the fit or to find optimal parameters), adjusts where necessary and repeats the process.

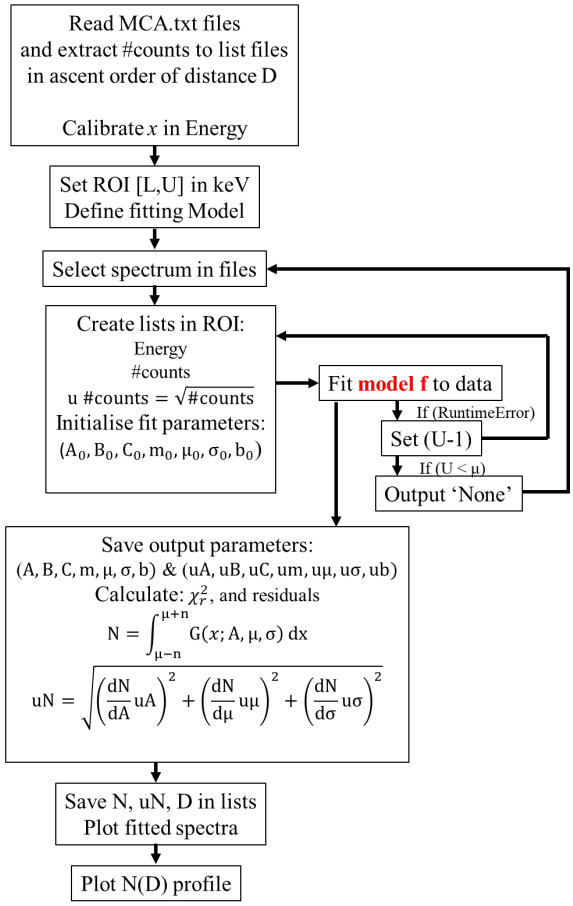

Fig. 3. A flowchart of the spectrum fitting process including the data flow.

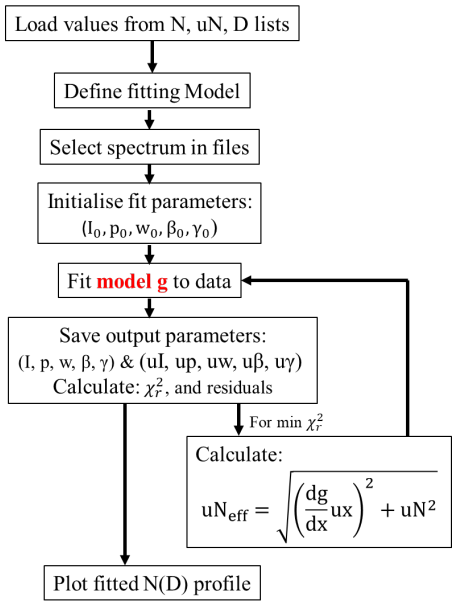

Fig. 4. A flowchart of the depth profile fitting process.

The ROI may be adjusted by reducing U by one channel to a lower energy until it equals to μ (the centroid of the Gaussian). If the process still fails to fit the data, an error message is registered (since effectively no photopeak is detected) and the method moves on to the next position. Following the fitting process, Equation 5 is used to calculate the total number of counts N_i corresponding to number of counts under the photopeak, i.e., indicative of the level of caesium-137 662 keV γ rays detected at each position i.

The aim of the fitting process is to find values of unconstrained parameters based on a minimization using a Lenvenberg-Marquardt algorithm. In python™ this is performed by the function scipy.optimize.curve_fit(); a chi-squared test of independence is used to assess the consistency of a given fit.

V. Results and Discussion

The γ-ray spectra obtained with caesium-137 at P1, and with the BLP prototype positioned at specific distances 30 up to 130 cm from the top-pipe, are shown in Fig. 5. This illustrates that the intensity of the 662 keV photopeak is greater when the detector is close to the source and decreases when it is further away, as expected, with the highest intensity observed at the shortest possible source-detector separation. A wide scatter continuum is observed due to effect of the surroundings and incomplete photon absorption in the detector crystal.

The sum of counts may be obtained by direct summation or by fitting an analytical function to the data. A Gaussian with an additional component to represent the low-energy tailing on the peak, f, was used, as per (1), with parameters as defined earlier. The χ_ν^2 for the fits were ~1 but the algorithm fails to fit peaks of small amplitude (< 15 counts). This error arises from the failure of the optimisation algorithm to achieve convergence within the specified number of iterations and may be attributable to the model's complexity and the presence of noise on a low amplitude photopeak. Note: applying moderate smoothing techniques, such as the Savitzky-Golay filter [19], on spectra with low photopeak

amplitudes prior to optimisation process may address this issue and, consequently, enhance the accuracy of the profile encompassing the limits of the γ-ray depth profile (not done in this work). Fig. 6 is an example of a fit for caesium-137. The number of counts under the photopeak N_p were extracted by integrating the Gaussian component of the optimized function (1), between 3σ on either side of the μ-peak value, plotted against the detector position in the blind-tube testbed, as per Fig. 6. These data describe an asymmetric point-spread function akin to astrophysical problems and have been fitted with a Moffat function, g, with a skew component, as per (7), where the parameters are as defined earlier. Fig. 6 suggests an acceptable fit incorporating the asymmetric trend, that is superior when compared to Gaussian-type models (see Table I).

The amplitude term, I, can be used to estimate the activity or concentration of caesium-137 in the sample, provided that a calibration is performed. The maximum peak height observed in this work was (15024 ± 119) cph (~4 cps) for a ^{137}Cs point source of activity of 304 kBq.

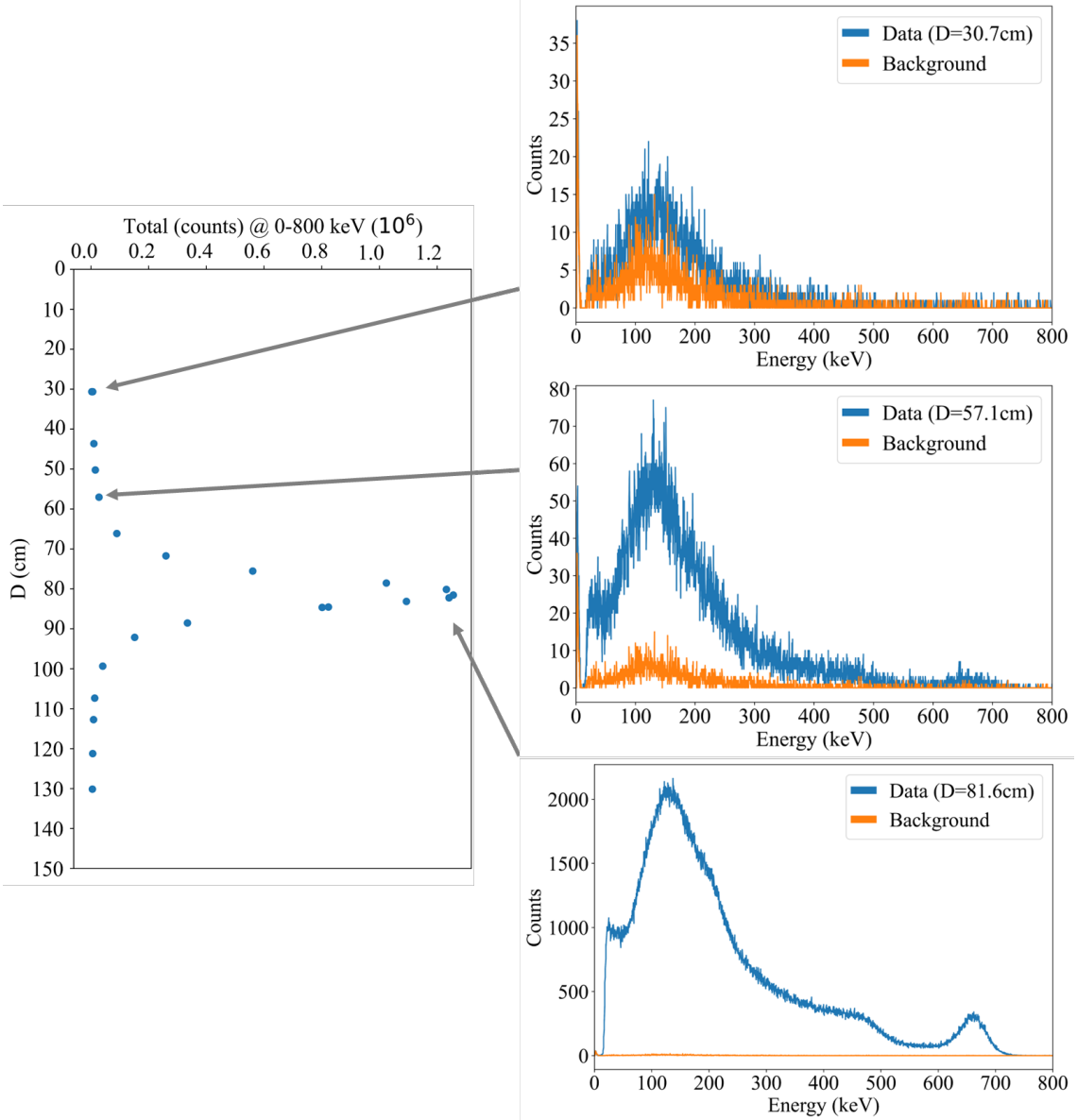

Fig. 5. Depth versus total counts for a single profile exercise (*left*), and example spectra for three different positions (*right*): 30.7 cm, 57.1 cm and 81.6 cm.

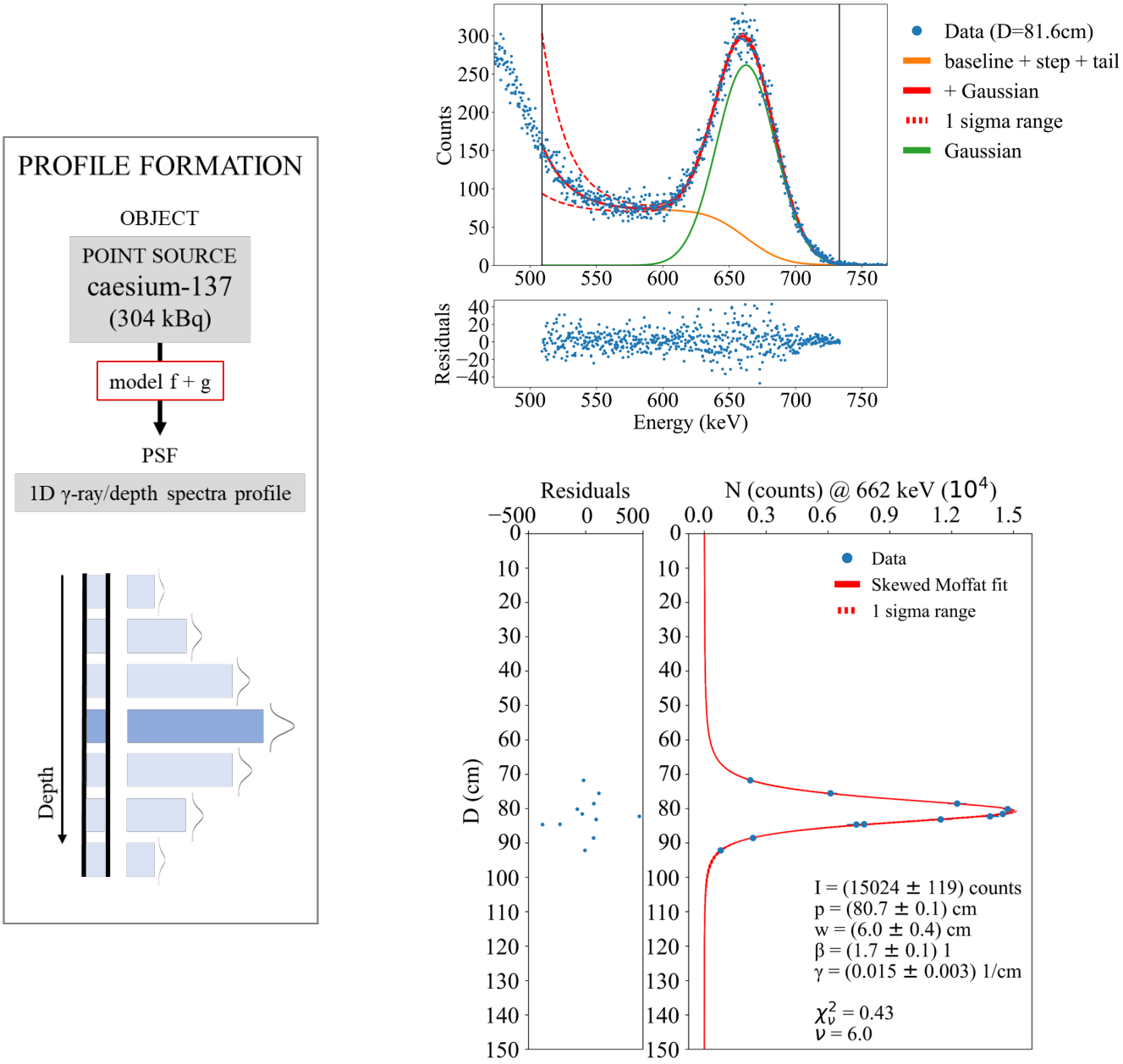

Fig. 6. A schematic of the depth profiling process (*left*) with an example spectrum (*right, top*) including the combination of fits comprising equation (1), and the depth profile obtained from an experimental scan (*right, bottom*) with the modified Moffat PSF fit as per equation (7), with the corresponding fit parameters: I represents the amplitude, p is the peak depth position, w refers to the width, β to the shape, and γ the skewness term of the profile. The reduced chi-squared, χ^2_ν, was 0.43, with the number of degrees of freedmon (ν) of 6.

The position of the source is inferred from the fit in Fig. 6 associated with the centroid parameter, p, to give (80.7 ± 0.1) cm. P1 was positioned at (79.8 ± 0.5) cm, highlighting a consistent result within the uncertainties (relative error ~1%).

The width term w, obtained can be used to estimate the vertical spatial resolution of the system defined at 50% of the signal, and given approximately by $2w_x\sqrt{2^{1/\beta}-1}$, i.e, (8.5 ± 0.6) cm.

The shape terms β and γ determine the rate of change of the width of the distribution (spread of radiation) in relation to the peak position p along the x-axis. These suggest a relative degree of attenuation that photons experience before reaching the sensor, influenced by factors such as shielding or the density of the surrounding media. Since in this study the setup was designed to minimize attenuation, the values obtained correspond to this scenario, as per, (1.7 ± 0.1) and (0.015 ± 0.003) cm^{-1} for β and γ respectively, and are intrinsic to this blind-tube test bed and detector system arrangement. Moreover, the γ value obtained is positive, very small but non-zero, indicating a slight asymmetry in the distribution (steeper on the right side of the peak centroid than the left). This effect may be due to an asymmetric attenuation, i.e., presence of sensor case, electronics, and the length of the probe case where the MCA is positioned, on the back of the sensor crystal.

TABLE I
POINT SPREAD FUNCTION MODELS AND FIT PARAMETERS

Parameter	Gaussian	Skewed Gaussian	1-D Moffat	1-D Skew Moffat
A / counts	14493 ± 397	11806 ± 1569	14924 ± 209	15024 ± 119
μ / cm	80.5 ± 0.3	78 ± 1	80.5 ± 0.1	80.7 ± 0.1
σ / cm	4.3 ± 0.2	5.3 ± 0.7	7.1 ± 0.8	6.0 ± 0.4
β	-	-	2.2 ± 0.3	1.7 ± 0.1
γ / cm^{-1}	-	1.0 ± 0.5	-	0.015 ± 0.003
χ^2_ν	12.8	12.5	1.7	0.4
df	8	7	7	6

By analyzing the parameters (I, p, w, β) and their corresponding 3-standard deviations in both non-skewed and skewed Moffat models (Table I), the results indicate that all the corresponding parameters are similar within the 99.7% confidence range. This implies that the models yield similar fits to the data distribution, which is reasonable given that the obtained γ value is close to zero.

VI. CONCLUSION

In-situ borehole monitoring of radioactivity is an important modality by which both the location and the composition of radioactive contamination entrained in groundwater and geological strata can be probed. However, photon spectra arising from this approach can be complex and varied, and hence reliable analytical methods are necessary by which individual contributions to them can be estimated. Likewise, the point-spread distribution of photon count data that can arise with depth concerning a particular anomaly can be asymmetric due to inhomogeneities in the borehole surroundings and the influence of the monitoring instrumentation on scatter whilst in use underground.

In this research, the design and development of a prototype borehole monitoring probe and bespoke testbed has been described. The use of these is demonstrated in which the semi-empirical model developed by Phillips et al. [9] has been combined with a development of the Moffat PSF [13] to extract spectroscopic features and localization information, respectively. This approach, combined with the ABACUS BLP, yields a consistent indication of the depth of radioactive source positioned in a bespoke, blind-tube testbed. In future, these approaches will be targeted towards understanding more complicated source distribution scenarios, the proportion and spatial distribution of ^{137}Cs and ^{90}Sr in aqueous media and progressing to active testing in the field.

GLOSSARY

A Amplitude of Gaussian function applied to photopeak.
B Amplitude of step function expressed as a fraction of A.
b An offset representing the residual background count.
β Parameter governing the shape of a depth profile.
C Tail function amplitude expressed as a fraction of A
df Number of degrees of freedom.
f Spectrum fitting function.
G Gaussian function.
g Moffat point-spread function (PSF).
γ Skew parameter of the peak of a depth profile.
I The amplitude of a Moffat PSF.
μ Centroid of the Gaussian function applied to photopeak.
m The slope of the exponential in the tail function, T.
N Number of counts in photopeak.
n Constant in Gaussian integral ensuring 3σ coverage.
p Peak depth position as per centroid components below.
p_x Denotes the centroid in x of an image or depth profile.
p_y Denotes the centroid in y of an image or depth profile.
S Step discontinuity function in photon spectrum.
s Sigmoid-type function describing x-axis asymmetry.
σ Standard deviation of the Gaussian applied to photopeak.
T Tail function applied to photon spectrum.
w_x Parameter governing the width of a depth profile in x.
w_y Parameter governing the width of a depth profile in y.
x_0 Central x coordinate of an elliptic profile.
y_0 Central y coordinate of an elliptic profile.
x The abscissa denoting photon energy or depth.
y Denotes parameter orthogonal to depth in Moffat PSF.

ACKNOWLEDGMENT

We acknowledge useful discussions with B. Greenhalgh and T. Calverley.

REFERENCES

[1] P. Hallington, J. Heneghan and J. Graham, (2021) "RemPlex Summit Case Studies: Optimization of Remediation Planning Approaches Based on Lessons Learned at the Sellafield Site, UK". Accessed 04 May 2022 https://www.pnnl.gov/projects/remplex/case-studies#CaseStudy4>.
[2] J. Homilius and S. Lorch, "On the theory of gamma ray scattering in boreholes", Geophys. Pros. 6 (4) pp. 342-364, 1958.
[3] H. L. Nguyen, C. de Fouquet, C. Courbet, R. Gurriaran, V. Kashparov, S. Levchuk and E. Barker, "Analysis of the relationship binding in situ gamma count rates and soil sample activities: Implication on radionuclide inventory and uncertainty estimates due to spatial variability", J. Env. Radio. vol. 192, pp. 349-361, 2018.
[4] R. D. Wilson, "Spectral shape analysis for contaminant logging at the Hanford site", IEEE Trans. Nucl. Sci. vol. 45 (3-1), pp. 997-1001, 1998.
[5] J. R. Giles and K. J. Dooley, "High resolution gamma-spectroscopy well logging system", J. Radio. Nucl. Chem. vol. 233, pp. 125b-130, 1998.
[6] C. J. Koizumi, J. R. Brodeur, R. K. Price, J. E. Meisner and D. C. Stromswold, "High-resolution gamma-ray spectrometry logging for contamination assessment", Nucl. Geophys. vol. 8 (2), pp. 149-164, 1994.

[7] L. L. Gadeken, Wm. P. Madigan and H. D. Smith Jr., "Radial distributions of ^{60}Co contaminants surrounding wellbores at the Hanford site", IEEE Nucl. Sci. Symp. vol. 1, pp. 214-218, 1995.

[8] S. Elísio and M. J. Joyce, "Method and apparatus for determining attributes of a source of radiation," Patent P347121GB/CAB. 29, Sept. 2022.

[9] G. W. Phillips and K. W. Marlow, "Automatic analysis of gamma-ray spectra from germanium detectors", Nucl. Inst. Meth. vol. 137 (3), pp. 525-536, 1976.

[10] J. Uher, G. Roach, and J. Tickner, "Peak fitting and identification software library for high resolution gamma-ray spectra", Nucl. Inst. Meth. vol. A619 (1-3), pp. 457-459, 2010.

[11] P. Mortreau and R. Berndt, "Characterisation of cadmium zinc telluride detector spectra - application to the analysis of spent fuel spectra", Nucl. Inst. Meth. vol. A458 (1-2), pp. 183-188, 2001.

[12] A. Varley, A. Tyler, L. Smith and P. Dale, "Development of a neural network approach to characterise ^{226}Ra contamination at legacy sites using gamma-ray spectra taken from boreholes", J. Env. Radio. vol. 140, pp. 130-140, 2015.

[13] A. F. J. Moffat, "A theoretical investigation of focal stellar images in the photographic emulsion and application to photographic photometry", Ast. and Astro., vol. 3, pp. 455, 1969.

[14] T. M. Ryan, A. J. Hinojosa, R. Vroman, C. Papasavvas and L. Lagnado, "Correction of z-motion artefacts to allow population imaging of synaptic activity in behaving mice", J. Physiol., vol. 598 (10), pp. 1809-1827, 2020.

[15] G. Fiorentino, I. Ferraro, G. Iannicola, G., Bono, M. Monelli, V. Testa, C. Arcidiacono, M. Faccini, R. Gilmozzi, M. Xompero and R. Briguglio, "On the use of asymmetric PSF on NIR images of crowded stellar fields", In Adaptive Optics Systems IV, vol. 9148, pp. 1301-1314, 2014.

[16] S. K. Jensen Jr, S. D. Brittain, J. R. Najita and J. S. Carr, "Modeling of CO Rovibrational Line Emission of HD 141569", Pub. Astron. Soc. Pac., vol. 133, 104402, 2021.

[17] J. P. Dedieu, Newton-Raphson Method. In: Engquist, B. (eds) Encyclopedia of Applied and Computational Mathematics. Springer, Berlin, Heidelberg, 2015.

[18] S. Elísio, M. J. Joyce, J. Graham, and B. Greenhalgh, "An advanced blind-tube monitoring instrument to improve characterization of subsurface radioactive plumes," in EPJ Web of Conferences, (2021) vol. 253, pp. 08005, 2021.

[19] A. Savitzky and M. J. E. Golay, "Smoothing and Differentiation of Data by Simplified Least Squares Procedures", Anal. Chem. 36 (8), 1627-1639, 1964.